Engineering 3 (2017) 136–143

Contents lists available at ScienceDirect

Engineering

journal homepage: www.elsevier.com/locate/eng

Research
Climate Change—Article

Multidecadal Trends in Large-Scale Annual Mean SATa Based on CMIP5 Historical Simulations and Future Projections

Nan Xing [a,b,c], Jianping Li [a,c,*], Lanning Wang [a,c]

[a] College of Global Change and Earth System Science, Beijing Normal University, Beijing 100875, China
[b] Beijing Meteorological Observatory, Beijing 100089, China
[c] Joint Center for Global Change Studies, Beijing 100875, China

ARTICLE INFO

Article history:
Received 1 February 2016
Revised 12 May 2016
Accepted 25 August 2016
Available online 29 November 2016

Keywords:
Surface air temperature anomalies (SATa)
Multidecadal trend
Coupled Model Intercomparison Project Phase 5 (CMIP5)
Projection

ABSTRACT

Based on observations and Coupled Model Intercomparison Project Phase 5 (CMIP5) results, multidecadal variations and trends in annual mean surface air temperature anomalies (SATa) at global, hemispheric, and hemispheric land and ocean scales in the past and under the future scenarios of two representative concentration pathways (RCPs) are analyzed. Fifteen models are selected based on their performances in capturing the temporal variability, long-term trend, multidecadal variations, and trends in global annual mean SATa. Observational data analysis shows that the multidecadal variations in annual mean SATa of the land and ocean in the northern hemisphere (NH) and of the ocean in the southern hemisphere (SH) are similar to those of the global mean, showing an increase during the 1900–1944 and 1971–2000 periods, and flattening or even cooling during the 1945–1970 and 2001–2013 periods. These observed characteristics are basically reproduced by the models. However, SATa over SH land show an increase during the 1945–1970 period, which differs from the other hemispheric scales, and this feature is not captured well by the models. For the recent hiatus period (2001–2013), the projected trends of BCC-CSM1-1-m, CMCC-CM, GFDL-ESM2M, and NorESM1-ME at the global and hemispheric scales are closest to the observations based on RCP4.5 and RCP8.5 scenarios, suggesting that these four models have better projection capability in SATa. Because these four models are better at simulating and projecting the multidecadal trends of SATa, they are selected to analyze future SATa variations at the global and hemispheric scales during the 2006–2099 period. The selected multi-model ensemble (MME) projected trends in annual mean SATa for the globe, NH, and SH under RCP4.5 (RCP8.5) are 0.17 (0.29) °C, 0.22 (0.36) °C, and 0.11 (0.23) °C·decade^{-1} in the 21st century, respectively. These values are significantly lower than the projections of CMIP5 MME without model selection.

1. Introduction

Global climate models play an important role in improving our understanding of climate variability and its causes, and providing projections of future climate change. In order to conduct multimodel intercomparison on the basis of a unified framework, the World Climate Research Programme (WCRP) has coordinated the Coupled Model Intercomparison Project (CMIP) [1,2]. Based on CMIP experiments, comparative analyses of modeled and observed results help us to better understand the advantages and disadvantages of models in reproducing observed climate features; such analyses are also helpful in improving the models and the corresponding predictions of future climate change.

Under global warming, global surface air temperature anomalies (SATa) have exhibited warming with multidecadal variations since the 20th century. Previous studies indicated that the multidecadal variations in global mean SATa can be divided into two warming periods (1900s–1940s and 1970s–1990s) and two warming hiatus periods (1940s–1970s and 2000s–present day) [3,4]. The multidecadal trends of SATa in the northern hemisphere

* Corresponding author.
E-mail address: ljp@bnu.edu.cn

http://dx.doi.org/10.1016/J.ENG.2016.04.011

(NH) differ in strength from those in the southern hemisphere (SH) during the rapidly warming period (1979–2010) [5], indicating uneven characteristics in multidecadal variations of SATa at hemispheric scales. Moreover, the multidecadal variations in SATa at hemispheric scales display various influences on agriculture, ecological systems, and the economy [6]. Thus, the simulation and future projection of multidecadal changes in SATa are of great concern.

Many models are basically capable of capturing long-term warming trends and the temporal variations in observed SATa for the global and hemispheric means [7–9]. The characteristics of more long-term warming in SATa over land (NH) than over sea (SH) are also generally captured by historical simulations [10,11]. Moreover, the multidecadal warming trends (e.g., 1901–1950 and 1951–2010) for the global and hemispheric means have also been basically reproduced by many models [11]. However, there are comparatively few existing studies on assessments in SATa during the hiatus periods (1940s–1970s and 2000s–present day), and little research has been devoted to the evaluation of discrepancies in the multidecadal variations in SATa over hemispheric land and ocean and in future projections. Thus, further research is needed to evaluate the capacity of the CMIP5 models to reproduce the multidecadal trends at the global and hemispheric scales, as well as future projections. Moreover, although the projections in multi-model ensemble (MME) SATa are generally based on all available models, MME without the verification of model fidelity [12] may affect the reliability of future projections. The selection of models in order to obtain more reliable future projections is of great importance.

This paper focuses on multidecadal trends in global and hemispheric annual mean SATa in CMIP5 during the warming and warming hiatus periods. The remainder of the paper is organized as follows: In Section 2, we briefly introduce the CMIP5 models, the reanalysis data, and the methodology used in this study; Section 3 presents the results and discussion; and Section 4 provides a summary.

2. Datasets and methodology

2.1. Datasets

The coupled climate model outputs are taken from the CMIP5 multi-model data archive (http://cmip-pcmdi.llnl.gov/cmip5/index.html). In this study, the main focus is on 20th century historical experiments [13] and on the projection experiments under the representative concentration pathway (RCP) 4.5 and 8.5 scenarios [14] with the base period 1961–1990. RCP4.5 and RCP8.5 are defined such that the radiative forcing will reach about 4.5 $W{\cdot}m^{-2}$ and 8.5 $W{\cdot}m^{-2}$, respectively, by the year 2100. From the archive, we use monthly surface air temperature (SAT) data from 15 coupled models with one initial condition realization (r1i1p1) (Table 1). The models are primarily selected based on data availability, model diversity, and their performances in temporal variability, long-term trend, multidecadal variations, and trends of global annual mean SATa (figures not shown).

For model validation, we used one set of reanalysis monthly data from the Met Office Hadley Centre and the University of East Anglia's Climatic Research Unit, which comprises combined land and sea surface temperature, version 4 (HadCRUT4) [5], with a horizontal resolution of 5° × 5°. The dataset covers the period 1900–2013.

2.2. Methodology

In order to avoid influence from missing data or some singular points to linear fitting, a method of regression coefficients has been proposed, called Sen's slope estimator [15]. In this study, the linear trend and the corresponding confidence interval are calculated by Sen's estimator. In addition, the nonparametric Mann–Kendall test is used to assess the significance of the linear trend [16].

3. Results and discussion

3.1. Multidecadal variations and trends in annual mean surface air temperature anomalies (SATa) in observation

Fig. 1 shows the temporal evolutions and trends of annual mean SATa for the globe, NH and SH, hemispheric land, and hemispheric ocean during the 1900–2013 period. All hemispheric-scale annual mean SATa show a long-term warming with multidecadal variations, as well as larger interannual variations from the global mean. In recent years, SATa increase more in the NH than the globe, and less in the SH than the

Table 1
Models from Coupled Model Intercomparison Project Phase 5 (CMIP5) and the corresponding descriptions.

Model	Institution	Resolution (lat × lon)	Data period	
			His+ RCP4.5	His+ RCP8.5
BCC-CSM1-1-m	Beijing Climate Center, China Meteorological Administration	1.125° × 1.125°	1900–2099	1900–2099
BNU-ESM	Beijing Normal University	2.8° × 2.8°	1900–2099	1900–2099
CanESM2	Canadian Centre for Climate Modelling and Analysis	2.8° × 2.8°	1900–2099	1900–2099
CESM1-CAM5	National Center for Atmospheric Research	0.94° × 1.25°	1900–2099	1900–2099
CMCC-CM	Euro-Mediterranean Center on Climate Change	0.75° × 0.75°	1900–2099	1900–2099
CNRM-CM5	National Center for Meteorological Research	1.4° × 1.4°	1900–2099	1900–2099
GFDL-ESM2M	Geophysical Fluid Dynamics Laboratory	2.0° × 2.5°	1900–2099	1900–2099
GISS-E2-H	NASA Goddard Institute for Space Studies	2.0° × 2.5°	1900–2099	1900–2099
HadCM3	Met Office Hadley Centre	3.8° × 2.5°	1900–2005	1900–2005
IPSL-CM5A-MR	Institute Pierre Simon Laplace	1.27° × 2.5°	1900–2099	1900–2099
MIROC-ESM-CHEM	Japan Agency for Marine-Earth Science and Technology, Atmosphere and Ocean Research Institute (The University of Tokyo), and National Institute for Environmental Studies	2.8° × 2.8°	1900–2099	1900–2099
MPI-ESM-P	Max Planck Institute for Meteorology	1.865° × 1.875°	1900–2005	1900–2005
MRI-ESM1	Meteorological Research Institute	1.121° × 1.125°	1900–2005	1900–2005
NorESM1-ME, NorESM1-M	Norwegian Climate Centre	1.89° × 2.5°	1900–2099	1900–2099

globe, and show more warming over land than over ocean [11]. In addition, the long-term trend magnitude over NH land is greater than that over SH land. Similarly, the long-term trend magnitude over NH ocean is greater than that over SH ocean. Based on the multidecadal transit years in global annual mean SATa, the multidecadal variations are divided into two warming periods (1900–1944 and 1971–2000) with significant increasing trends and two hiatus periods (1945–1970 and 2001–2013) with weaker trends, as shown in Fig. 1(g). Compared to the global mean, similar multidecadal variations over NH land as well as over NH and SH oceans are found, but with different trend magnitudes. However, SATa over SH land show an increasing trend (0.06 °C·decade^{-1}) during the 1945–1970 period, which is different from the global trend and from other hemispheric scales (Table 2). Among NH land and NH and SH oceans, changes in trend magnitudes over NH land are the largest during the four periods. The trend over NH land is 0.3 °C·decade^{-1} during the 1971–2000 period, and decreases to 0.05 °C·decade^{-1} during the 2001–2013 period, indicating the warming hiatus in the latter period.

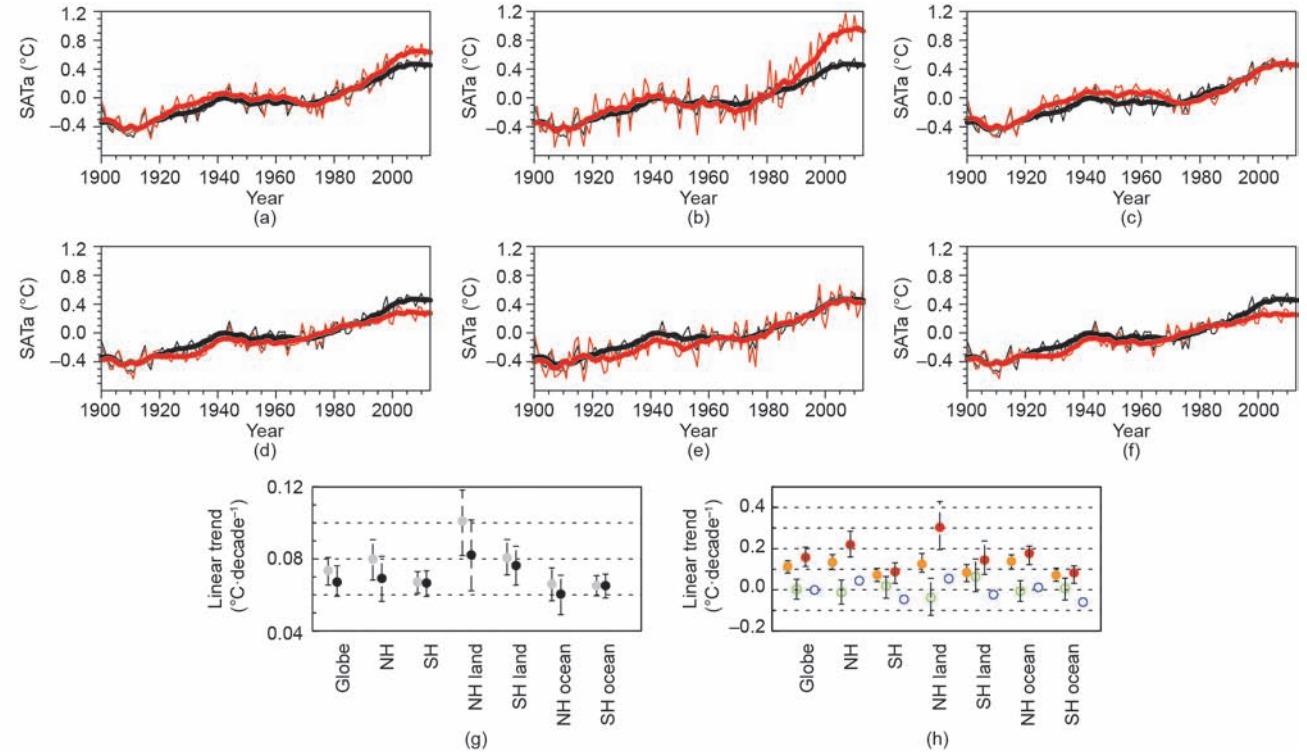

Fig. 1. (a–f) Time series and (g, h) linear trends (°C·decade^{-1}) of weighted annual mean surface air temperature anomalies (SATa) over the globe, northern hemisphere (NH), southern hemisphere (SH), land in the NH and SH, and oceans in the NH and SH since 1900. (a) NH; (b) NH land; (c) NH ocean; (d) SH; (e) SH land; (f) SH ocean; (g) long-term trend; (h) multidecadal trend. (a–f) The black and red solid lines represent the globe and each hemispheric scale, respectively; the thin and thick lines denote the raw time series and decadal variability obtained from the 11-year running average, respectively. (g) The gray and black circles represent the 1900–2005 and 1900–2013 periods, respectively. (h) The orange, green, red, and blue circles denote the 1900–1944, 1945–1970, 1971–2000, and 2001–2013 periods, respectively. (g, h) The solid (hollow) circle indicates significant (insignificant) at a 95% confidence level; error bars show the 95% confidence interval, and the dashed lines are scale marks.

Table 2
Observed SATa trends in the globe, NH, SH, land in the NH and SH, and oceans in the NH and SH for different periods.

	Trend (°C·decade^{-1})					
	1900–2013	1900–2005	1900–1944	1945–1970	1971–2000	2001–2013
Globe	**0.074** (0.07, 0.08)	**0.067** (0.06, 0.08)	**0.11** (0.08, 0.14)	0 (−0.05, 0.05)	**0.16** (0.11, 0.21)	0 (−0.02, 0.02)
NH	**0.080** (0.07, 0.09)	**0.070** (0.06, 0.08)	**0.13** (0.10, 0.17)	−0.01 (−0.07, 0.05)	**0.22** (0.16, 0.28)	0.04 (0, 0.80)
SH	**0.067** (0.06, 0.07)	**0.067** (0.06, 0.07)	**0.07** (0.04, 0.10)	0.02 (−0.04, 0.06)	**0.09** (0.03, 0.13)	−0.05 (−0.09, −0.01)
NH land	**0.100** (0.08, 0.12)	**0.080** (0.06, 0.1)	**0.12** (0.08, 0.18)	−0.04 (−0.12, 0.06)	**0.30** (0.19, 0.43)	0.05 (0.02, 0.09)
SH land	**0.080** (0.07, 0.09)	**0.080** (0.07, 0.09)	**0.08** (0.04, 0.12)	0.06 (−0.01, 0.15)	**0.14** (0.07, 0.24)	−0.02 (−0.17, 0.07)
NH ocean	**0.066** (0.06, 0.08)	**0.060** (0.05, 0.07)	**0.14** (0.10, 0.17)	−0.01 (−0.06, 0.04)	**0.18** (0.12, 0.21)	0.01 (−0.02, 0.05)
SH ocean	**0.065** (0.06, 0.07)	**0.065** (0.06, 0.07)	**0.07** (0.04, 0.10)	0.01 (−0.05, 0.06)	**0.08** (0.03, 0.12)	−0.06 (−0.08, −0.01)

Bold type indicates a trend that is significant at a 95% confidence level. The range in brackets indicates the 95% confidence interval.

3.2. Multidecadal variations and trends in model-simulated SATa and future projections

Annual mean SATa over the global and hemispheric scales from the 15 CMIP5 models and the MME are shown in Fig. 2. The model results present a large spread. The MME SATa over the global and hemispheric means are comparable to historical observations, but have smaller interannual variations, as shown in Fig. 2(a)–(g). The multidecadal trends in the global mean SATa of MME during the first three periods further indicate that the models are basically capable of reproducing the temporal shape for the global mean, as shown in Fig. 2(h)–(k); this result is consistent with previous research [11]. For hemispheric scale, the multidecadal variations can also be basically reproduced by the models, except for SH land, where the modeled SATa show a decreasing trend during the 1945–1970 period, as shown in Fig. 2(j). In addition, most hemispheric scales show a trend within the 95% confidence level of the observed trend during the two warming periods (1900–1944 and 1971–2000), except for NH and SH oceans, as shown in Fig. 2(i) and (k). It is seen that the trend magnitudes over the NH and SH oceans are less than the observed magnitudes during the 1900–1944 period, resulting in the underestimation of modeled long-term trends over the SH and the globe, as shown in Fig. 2(h). In addition, Jones et al. [11] pointed out that many models could capture the multidecadal variations in global mean SATa, and further evaluated the global trends during the 1901–2010, 1901–1950, 1951–2010, and 1979–2010 periods. By contrast, it is found that oceans in which the trend magnitudes are underestimated mainly concentrate in the northern Pacific and Atlantic during the 1900–1944 period, and oceans in which the trend magnitudes are overestimated are mainly located in the SH tropical Pacific and Southern Ocean during the 1971–2000 period. In addition to the warming periods, the characteristics of trends at the hemispheric scale are also analyzed during the hiatus period (1945–1970), and an interesting feature is found. Warming encompasses the SH land, a finding that is not simulated by the models.

Based on the above evaluation of multidecadal trends in large-scale annual mean SATa, it is found that the models can basically reproduce the multidecadal variations in SATa during the 1900–2005 period. Furthermore, global mean SATa show a hiatus since the 21th century [3,4]. How do the models project variations in SATa at global and hemispheric scales during this hiatus period? To answer this question, we will project the hemispheric SATa under the medium-low emissions scenario of RCP4.5 and the high emissions scenario of RCP8.5. The future projection datasets of HadCM3 only cover the 2006–2035 period, and the data from

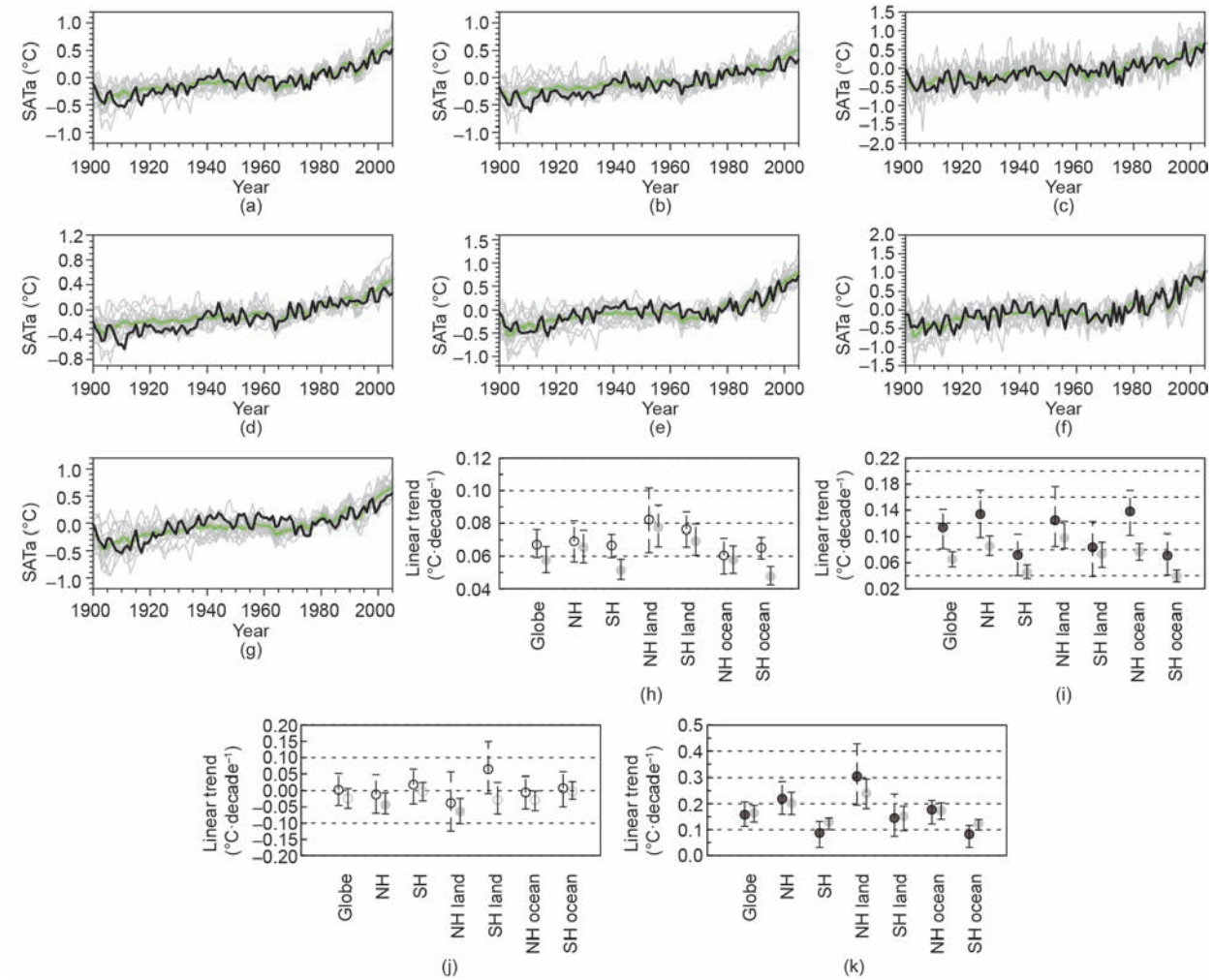

Fig. 2. Time series of weighted annual mean SATa of the (a) globe, (b) NH, (c) SH, (d) NH land, (e) SH land, (f) NH ocean, and (g) SH ocean from the models (gray lines), multi-model ensemble (MME) mean (green lines), and HadCRUT4 reanalysis data (black lines) from 1900 to 2005. Linear trends (°C·decade^{-1}) in weighted annual mean SATa from the MME of the 15 CMIP5 models (the gray circle) and observation data (the black circle) during (h) 1900–2005, (i) 1900–1944, (j) 1945–1970, and (k) 1971–2000. The hollow and solid circles, error bars, and dashed lines have the same meanings as in Fig. 1.

MPI-ESM-P and MRI-ESM1 were unavailable at the time of writing, so these three models were omitted from our RCP analysis.

Fig. 3 shows the linear trends in annual mean SATa for RCP4.5 and RCP8.5 for the 2001–2013 period. The trends of the global and hemispheric mean vary greatly from one model to another. It is obvious that most models overestimate the trends for the hemispheric scales, and a similar result is seen for the global scale [6]. By comparison, the SATa trends of BCC-CSM1-1-m, CMCC-CM, GFDL-ESM2M, and NorESM1-ME are closest to the observed trends. Previous studies indicate that changes in global SATa are jointly influenced by increasing anthropogenic greenhouse gas, internal climate variability, and so on [2]. The overestimation of anthropogenic forces, different sensitivities to external forces of models, and inconsistent model capabilities in reflecting internal climate variability are possible reasons for the widely different and overestimated trends at the hemispheric and global scales during the 2001–2013 period [2,7,18]. This issue needs to be further discussed in future.

The result in Fig. 3 indicates that the models of BCC-CSM1-1-m, CMCC-CM, GFDL-ESM2M, and NorESM1-ME show better projection capability during the 2001–2013 period. Hence, the simulation abilities of these four models are evaluated according to their multidecadal trends at the global and hemispheric scales during different periods (Table 3). As can be seen, the performance in reproducing multidecadal variations differs among the four models on hemispheric scales. Compared with historical observations (Table 2), the characteristics of the global mean are best represented by the four models during the four periods, and the trends for the global and hemispheric means of these four models are closest to the observed trends during the 1945–1970 and 1971–2000 periods. For the 1900–1944 period, like the MME results shown in Fig. 2(g), the four models give similar trends but with less trend magnitudes at the global and hemispheric scales. In general, the four models can mostly reproduce the temporal shape at the global and hemispheric scales. Due to these models' capability in simulating and projecting the multidecadal trends of SATa, we selected them for analyzing future SATa variations during the 2006–2099 period.

Fig. 4 shows the changes in annual mean SATa of the MME over the global and the hemispheric scales from BCC-CSM1-1-m, CMCC-CM, GFDL-ESM2M, and NorESM1-ME for the 2006–2099 period under RCP4.5 and RCP8.5. For the globe and for each hemispheric scale, SATa show an overall increase in the future. However, SATa increase more over the NH (land, ocean) than over the SH (land, ocean) under both scenarios, and linear trends are larger under the high emissions scenario of RCP8.5 than under the medium-low emissions scenario of RCP4.5 during the 2006–2099 period. Moreover, for the global and hemispheric scales, SATa show a linear increase under RCP8.5 since 2006, and the increase in SATa is greater under RCP8.5 than under RCP4.5 starting about 2020. On the other hand, SATa reach a peak around 2080 and then do not increase under RCP4.5. Variations of SATa under RCP8.5

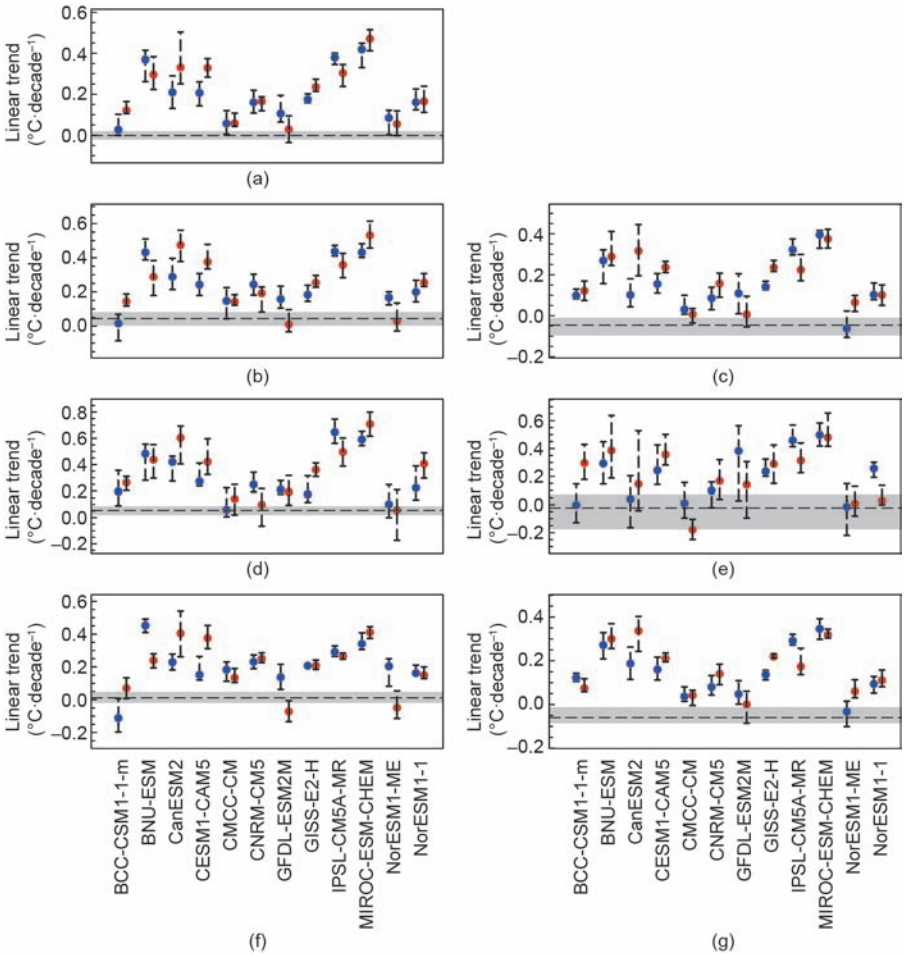

Fig. 3. Weighted linear trend (°C·decade^{-1}) in the models for the (a) globe, (b) NH, (c) SH, (d) NH land, (e) SH land, (f) NH ocean, and (g) SH ocean from 2001 to 2013 under RCP4.5 (blue circles) and RCP8.5 (red circles). The dashed line indicates the value of the trend from HadCRUT4 reanalysis, and the shaded area covers the 50% confidence interval. Error bars show the 50% confidence interval for each model.

Table 3
Modeled SATa trends in the globe, NH, SH, land in the NH and SH, and oceans in the NH and SH for different periods.

Period	Model	Trend (°C·decade^{-1})						
		Globe	NH	SH	NH land	SH land	NH ocean	SH ocean
1900–2005	BCC-CSM1-1-m	0.07	0.11	0.04	0.14	0.07	0.10	0.04
	CMCC-CM	0.05	0.05	0.06	0.07	0.09	0.03	0.06
	GFDL-ESM2M	0.05	0.07	0.02	0.09	0.03	0.07	0.02
	NorESM1-ME	0.05	0.05	0.05	0.06	0.06	0.05	0.04
1900–1944	BCC-CSM1-1-m	0.02	0.12	−0.07	0.16	−0.03	0.09	−0.07
	CMCC-CM	0.01	−0.02	0.04	−0.01	0.04	−0.02	0.03
	GFDL-ESM2M	0.02	0.07	−0.02	0.08	−0.02	0.07	−0.02
	NorESM1-ME	0.08	0.08	0.07	0.12	0.08	0.07	0.07
1945–1970	BCC-CSM1-1-m	0.02	−0.04	0.06	−0.08	0.04	0	0.07
	CMCC-CM	0.01	0.02	−0.01	0.02	0.12	0.01	−0.03
	GFDL-ESM2M	−0.08	−0.10	−0.06	−0.12	−0.16	−0.07	−0.04
	NorESM1-ME	−0.01	0.05	−0.09	0.07	−0.12	0.05	−0.08
1971–2000	BCC-CSM1-1-m	0.20	0.21	0.21	0.24	0.21	0.17	0.21
	CMCC-CM	0.18	0.24	0.10	0.32	0.11	0.21	0.10
	GFDL-ESM2M	0.15	0.21	0.11	0.26	0.11	0.17	0.11
	NorESM1-ME	0.10	0.07	0.14	0.06	0.15	0.08	0.14

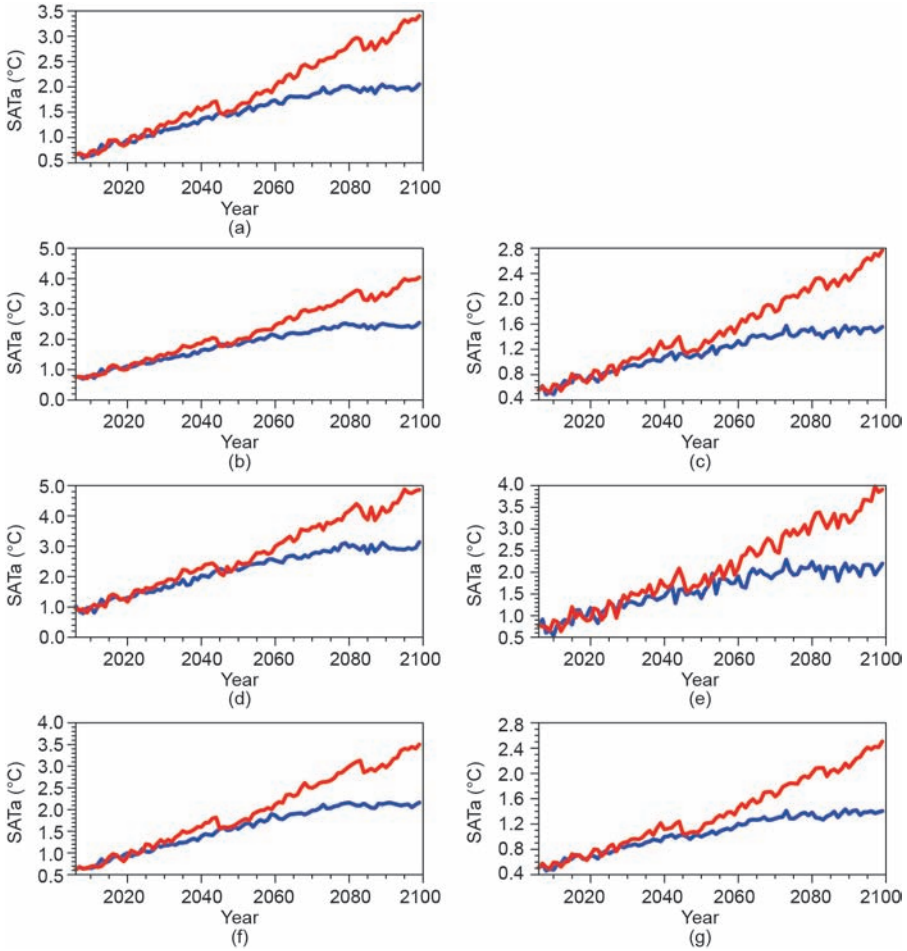

Fig. 4. Projected (2006–2099) time series of annual mean SATa for the globe and for each hemispheric scale based on the MME of the four CMIP5 models (BCC-CSM1-1-m, CMCC-CM, GFDL-ESM2M, and NorESM1-ME) under RCP4.5 (blue lines) and RCP8.5 (red lines). (a) Globe; (b) NH; (c) SH; (d) NH land; (e) SH land; (f) NH ocean; (g) SH ocean.

and RCP4.5 are closely related to variations of global anthropogenic radiative forcing for the two scenarios [14]. The different emissions of global anthropogenic forces are a possible reason for the distinct divergence in SATa under the two scenarios.

In addition, the trends in annual SATa for the globe, NH, SH, NH land, SH land, NH ocean, and SH ocean under RCP4.5 are 0.17, 0.22, 0.11, 0.26, 0.16, 0.19, and 0.10 °C·decade^{-1}, respectively, and are significantly less than those under RCP8.5 (0.29, 0.36, 0.23, 0.43, 0.33, 0.31, and 0.21 °C·decade^{-1}, respectively; figure not shown). Moreover, the trends in annual SATa from the MME results of the 12 models for the globe, NH, SH, NH land, SH land, NH ocean, and SH ocean under RCP4.5 (RCP8.5) are 0.20 (0.41), 0.24 (0.49), 0.15 (0.33),

0.29 (0.58), 0.21 (0.45), 0.21 (0.42), and 0.14 (0.30) °C·decade^{-1} (figures not shown). The projected trends at the global and hemispheric scales with model selection are clearly lower than the MME results of the 12 models and the results without model selection in the previous study [19] under RCP4.5 and RCP8.5. Moreover, both years (2063 and 2053) in which global warming reaches 2 °C under the two scenarios occur later than in the MME (2047 and 2038) without model selection when using the same base period [19]. The results at hemispheric scales are similar to the global mean.

3.3. Discussion

CMIP5 models perform well in simulating the long-term trends of SATa [2]; however, the performance in reproducing the multidecadal variations of SATa differs among the models. It can be seen from Fig. 5 that some models, including FGOALS-g2, FIO-ESM, GFDL-CM2p1, GISS-E2-R-CC, INMCM4, and MPI-ESM-LR, are not capable of reproducing the multidecadal variations in annual mean SATa for the globe, as well as for each hemispheric scale (Fig. 5(a)–(g)). Obviously, these models give increasing trends over the global and hemispheric means during the 1945–1970 period, indicating the overestimation of modeled trends during this period. In addition, during the 1900–1944 and 1945–1970 periods, the trend magnitudes of each hemispheric mean from these models are close to the long-term global mean, suggesting that the linear increase of SATa may be due to linear responses of these models to increasing anthropogenic greenhouse gases, and may be insufficient in simulating the internal climate variability that modulates the decadal variation in SATa [4,20–22] in these models. The result implies that the capabilities of these models in reproducing the internal climate variability may need to be improved.

4. Conclusions

In this study, we attempt to select relatively good model simulations before using MME results. Hence, 15 models are selected based on their ability to portray the temporal variability, long-term trends, and multidecadal trends of the global mean SATa. Then, using the 15 selected CMIP5 models, we further investigate the multidecadal trends in annual mean SATa at the global and hemispheric scales, and the future projection.

Results from the observations show that SATa over NH land, NH ocean, and SH ocean display similar multidecadal changes, while SATa over SH land show a warming trend during the 1945–1970 period. The models not only present certain capabilities in reproducing the multidecadal warming trends, which are consistent with previous studies [11], but also reproduce the cooling trend over NH land, NH ocean, and SH ocean during the hiatus period (1945–1970) well. However, the warming trend over SH

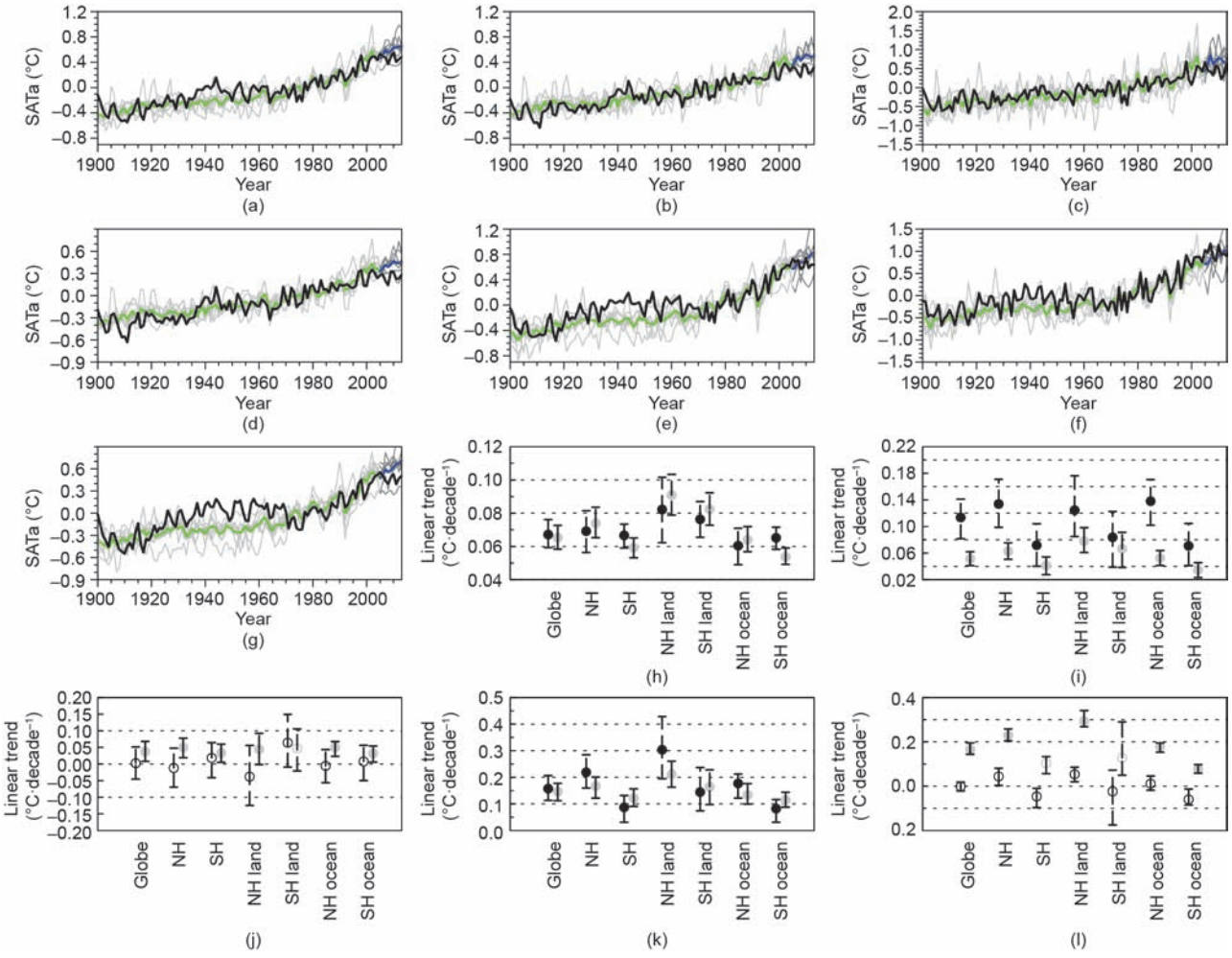

Fig. 5. As in Fig. 2, but for FGOALS-g2, FIO-ESM, GFDL-CM2p1, GISS-E2-R-CC, INMCM4, and MPI-ESM-LR from 1900 to 2013. The dark gray and blue lines represent the six models and their MME from 2006 to 2013 under RCP4.5. (a) Globe; (b) NH; (c) SH; (d) NH land; (e) SH land; (f) NH ocean; (g) SH ocean; (h) 1900–2005; (i) 1900–1944; (j) 1945–1970; (k) 1971–2000; (l) 2001–2013.

land cannot be well reproduced during the 1945–1970 period. In addition, although the models portray the warming trends over the NH and SH oceans during the 1900–1944 period, they underestimate the trend magnitudes, thus inducing an underestimation of modeled long-term trends of the NH, the SH, and the globe.

Furthermore, the projection capabilities of the models are evaluated based on RCP4.5 and RCP8.5 scenarios during the recent hiatus period (2001–2013). It is found that the trends reproduced by BCC-CSM1-1-m, CMCC-CM, GFDL-ESM2M, and NorESM1-ME at the global and hemispheric scales are closest to the observations, indicating better projection capability in SATa of these four models. Based on these models' performance in simulating multidecadal variations and trends in annual mean SATa (especially for the recent warming hiatus), we project the SATa variations by using the four models during the 2006–2099 period. The SATa projection of the global and hemispheric means from the four models shows an increase under both scenarios, but more increases under RCP8.5 than under RCP4.5. The warming trend magnitudes projected by the four models are apparently less than those of the MME of the CMIP5 models without model selection, and the occurrence years of 2 °C warming occur later under both scenarios as well [19].

In addition, we found that some models only give an increasing trend instead of the multidecadal variations in SATa for the global and hemispheric scales since the 20th century, implying that the capability of these models to reproduce the internal climate variability may need to be improved.

Acknowledgements

This study was supported by National Key Research and Development Program of China (2016YFA0601801), the State Key Program of National Natural Science Foundation of China (41530424), National Program on Global Change and Air-Sea Interactions, State Oceanic Administration (SOA) (GASI-IPOVAI-03), and the National Natural Science Foundation of China (41305121). We sincerely thank two anonymous reviewers whose comments improved the paper.

Compliance with ethics guidelines

Nan Xing, Jianping Li, and Lanning Wang declare that they have no conflict of interest or financial conflicts to disclose.

References

[1] Alley RB, Berntsen T, Bindoff NL, Chen Z, Chidthaisong A, Friedlingstein P, et al. Summary for policymakers. In: Solomon S, Qin D, Manning M, Chen Z, Marquis M, Averyt KB, et al., editors Climate change 2007: the physical science basis. Contribution of Working Group I to the Fourth Assessment Report of the Intergovernmental Panel on Climate Change. New York: Cambridge University Press; 2007. p. 1–18.
[2] Stocker TF, Qin D, Plattner GK, Tignor MMB, Allen SK, Boschung J, et al., editors. Climate change 2013: the physical science basis. Working Group I contribution to the Fifth Assessment Report of the Intergovernmental Panel on Climate Change. New York: Cambridge University Press; 2013.
[3] Knight J, Kennedy J, Folland C, Harris G, Jones GS, Palmer M, et al. Do global temperature trends over the last decade falsify climate predictions? B Am Meteorol Soc 2009;90(8):S22–3.
[4] Li J, Sun C, Jin FF. NAO implicated as a predictor of Northern Hemisphere mean temperature multidecadal variability. Geophys Res Lett 2013;40(20):5497–502.
[5] Morice CP, Kennedy JJ, Rayner NA, Jones PD. Quantifying uncertainties in global and regional temperature change using an ensemble of observational estimates: the HadCRUT4 data set. J Geophys Res 2012;117(D8):D08101.
[6] Dai A. Increasing drought under global warming in observations and models. Nat Clim Chang 2013;3(1):52–8.
[7] Ding Y, Ren G, Zhao Z, Xu Y, Luo Y, Li Q, et al. Detection, causes and projection of climate change over China: an overview of recent progress. Adv Atmos Sci 2007;24(6):954–71.
[8] Zhou T, Yu R. Twentieth-century surface air temperature over China and the globe simulated by coupled climate models. J Climate 2006;19(22):5843–58.
[9] Stott PA, Tett SF, Jones GS, Allen MR, Mitchell JF, Jenkins GJ. External control of 20th century temperature by natural and anthropogenic forcings. Science 2000;290(5499):2133–7.
[10] Knutson TR, Zeng F, Wittenberg AT. Multimodel assessment of regional surface temperature trends: CMIP3 and CMIP5 twentieth-century simulations. J Climate 2013;26(22):8709–43.
[11] Jones GS, Stott PA, Christidis N. Attribution of observed historical near-surface temperature variations to anthropogenic and natural causes using CMIP5 simulations. J Geophys Res 2013;118(10):4001–24.
[12] Shukla J, DelSole T, Fennessy M, Kinter J, Paolino D. Climate model fidelity and projections of climate change. Geophys Res Lett 2006;33(7):L07702.
[13] Taylor KE, Stouffer RJ, Meehl GA. An overview of CMIP5 and the experiment design. B Am Meteorol Soc 2012;93(4):485–98.
[14] Meinshausen M, Smith SJ, Calvin K, Daniel JS, Kainuma MLT, Lamarque JF, et al. The RCP greenhouse gas concentrations and their extensions from 1765 to 2300. Climatic Change 2011;109(1–2):213–41.
[15] Sen PK. Estimates of the regression coefficient based on Kendall's tau. J Am Stat Assoc 1968;63(324):1379–89.
[16] Mann ME. On smoothing potentially non-stationary climate time series. Geophys Res Lett 2004;31(7):L07214.
[17] Vial J, Dufresne JL, Bony S. On the interpretation of inter-model spread in CMIP5 climate sensitivity estimates. Clim Dynam 2013;41(11–12):3339–62.
[18] Kosaka Y, Xie SP. Recent global-warming hiatus tied to equatorial Pacific surface cooling. Nature 2013;501(7467):403–7.
[19] Zhang L, Ding Y, Wu T, Xin X, Zhang Y, Xu Y. The 21th century annual mean surface air temperature change and the 2 °C warming threshold over the globe and China as projected by the CMIP5 models. Acta Meteorol Sin 2013;71(6):1047–60. Chinese.
[20] Mochizuki T, Ishii M, Kimoto M, Chikamoto Y, Watanabe M, Nozawa T, et al. Pacific decadal oscillation hindcasts relevant to near-term climate prediction. Proc Natl Acad Sci USA 2010;107(5):1833–7.
[21] Meehl GA, Arblaster JM, Fasullo JT, Hu A, Trenberth KE. Model-based evidence of deep-ocean heat uptake during surface-temperature hiatus periods. Nat Clim Chang 2011;1(7):360–4.
[22] Sun C, Li J, Jin FF. A delayed oscillator model for the quasi-periodic multidecadal variability of the NAO. Clim Dynam 2015;45(7–8):2083–99.